Trends in Photochemistry & Photobiology
Vol. 22, 2023

Original Article

Site-specific investigation of DNA Holliday Junction dynamics and structure with 6-Methylisoxanthopterin, a fluorescent guanine analog

Zane Lombardo and Ishita Mukerji*

Department of Molecular Biology and Biochemistry, Molecular Biophysics Program, Wesleyan University, 52 Lawn Ave, Middletown, Connecticut 06459, USA.

ABSTRACT

DNA Holliday Junction (HJ) formation and resolution is requisite for maintaining genomic stability in processes such as replication fork reversal and double-strand break repair. If HJs are not resolved, chromosome disjunction and aneuploidy result, hallmarks of tumor cells. To understand the structural features that lead to processing of these four-stranded joint molecule structures, we seek to identify structural and dynamic features unique to the central junction core. We incorporated the fluorescent guanine analog 6-methylisoxanthopterin (6-MI) at ten different locations throughout a model HJ structure to obtain site-specific information regarding the structure and dynamics of bases relative to those in a comparable sequence context in duplex DNA. These comparisons were accomplished through measuring fluorescence lifetime, relative brightness, fluorescence anisotropy, and quenching assays. These time-resolved and steady-state fluorescence measurements demonstrate that the structural distortions imposed by strand crossing result in increased solvent exposure, less stacking of bases and greater extrahelical nature of bases within the junction core. The 6-MI base analogs in the junction reflect these structural changes through an increase in intensity relative to those in the duplex. Molecular dynamics simulations performed using a model HJ indicate that the primary sources of deformation are in the shift and twist parameters of the bases at the central junction step. These results suggest that junction-binding proteins may use the unique structure and dynamics of the bases at the core for recognition.

KEYWORDS: 6-MI, 6-Methylisoxanthopterin, Holliday junction, fluorescent guanine analog, DNA base dynamics.

ABBREVIATIONS

6-Methylisoxanthopterin (6-MI), Holliday Junction (HJ), Time-correlated single-photon counting (TCSPC), Root mean square deviations (RMSD), Root mean square fluctuations (RMSF), Molecular Dynamics (MD), Nuclear Magnetic Resonance (NMR), duplex-enhanced fluorescence (DEF), Assisted Model Building with Energy Refinement (AMBER).

INTRODUCTION

DNA Holliday junctions (HJs), branched molecules consisting of four double stranded arms, are essential intermediates for processes like replication fork reversal and double-strand break repair. Proper formation and resolution of DNA Holliday junctions must occur to maintain genomic stability during these important processes. Improper resolution of HJs can result in chromosome disjunction and aneuploidy leading to inherited genetic disorders

*Corresponding author: imukerji@wesleyan.edu

and cancer. There have been many studies investigating the overall structure and dynamics of the branched DNA molecule [1, 2] and how different proteins interact to resolve them [3, 4]. Single-molecule fluorescence and other studies have shown HJs primarily exist in two stacked anti-parallel conformational isomers, iso-I or iso-II, or an unstacked open conformation, with the stacked X isomers being favored in the presence of mono- and polyvalent cations [5-7]. The well-characterized J3 junction used in this study (Fig 1A) adopts the iso-II conformation 80% of the time, where B and R are the exchanging strands and H and X are the continuous strands [8-12]. The J3 junction is base pair matched with no homology, rendering it incapable of branch migration.

Although many studies have examined the structure and conformer distribution of HJs, there has been little investigation of the local structure and dynamics of DNA bases at the HJ core. Prior NMR studies have shown that bases at the junction center maintain Watson-Crick base pairing but deviate from a regular B-DNA conformation [13-15]. Importantly, the identity of bases at the core are critical for determining HJ conformer distribution and dynamics [16] and the core itself is the locus for many protein-HJ interactions [17-21]. Thus, understanding the structure and dynamics of the central bases is important for establishing junction

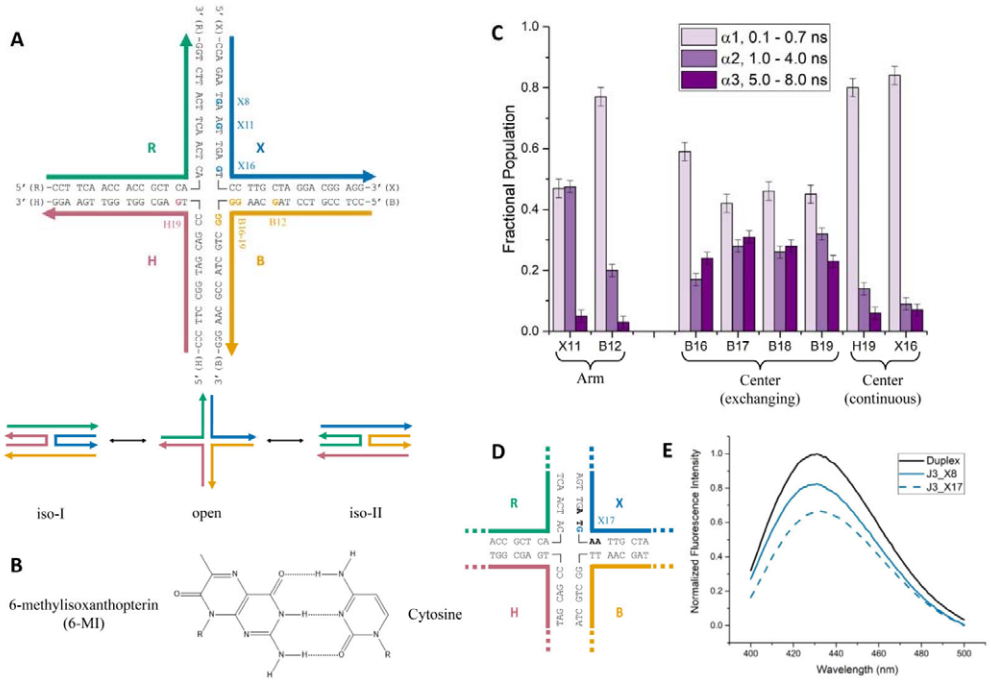

Fig. 1. 6-MI containing J3 Holliday junctions. (A) A schematic representation showing the J3 Holliday junction sequence and probe locations (bold and shown in strand color). Each experimental junction only contains one probe. The J3 HJ is detected in three possible conformations: iso-I, open, and iso-II; Iso-II is the preferred state (80%). (B) The chemical structure of the fluorescent guanine analog 6-MI, which forms Watson-Crick hydrogen bonds with cytosine. (C) Fractional populations of the lifetime components obtained from fitting decays to a sum of exponentials as described in the text. Mid- and long-range component populations increase in the junction center (B16-19) compared to the arms (X11, B12). (D) A schematic representation of the J3 junction sequence modified to incorporate the ATFAA or duplex-enhanced fluorescence sequence at the HJ core (Blue G is replaced with 6-MI). (E) Comparison of ATFAA sequence in junction and duplex DNA. Homoduplex DNA (HD, black) has the highest intensity, followed by ATFAA sequence incorporated in J3 arm (X8, blue) while the ATFAA sequence in the J3 center (X17, blue and dashed) has the lowest intensity. Samples contained 200 nM DNA in a 10 mM Tris, pH 7.5, 100 mM NaCl and 5 mM $MgCl_2$ buffer. Decay fit parameters are given in Supporting Information: Table S2.

behavior and how these repair and recombination intermediates interact with proteins.

To further investigate junction base structure and dynamics, we employed a fluorescent DNA base analog, 6-methylisoxanthopterin (6-MI), to report on local environment and motions at the level of a single DNA base. This fluorescent guanine analog forms Watson-Crick H-bonds with cytosine in double-stranded DNA while minimally perturbing normal structure (Fig. 1B) [22-24]. Previous studies have demonstrated that 6-MI fluorescence is sensitive to local environment within DNA, can measure the local motions of DNA bases in different sequence or structural contexts and sensitively reports on protein binding [22, 25-27]. Previously, 6-MI revealed significant differences in the local motion of DNA base mismatches, which could be related to the ability of the mismatch repair protein Msh2-Msh6 to recognize specific mismatch types [28]. Incorporated as a molecular sensor for G-quadruplexes, 6-MI fluorescence increases upon G-quadruplex formation as base stacking interactions are reduced [29, 30]. In this work, we used 6-MI to determine if the structure and dynamics of bases in different locations within the junction, particularly the junction center, were different and could lead to specific recognition by junction-binding proteins. We further examined if at the single base level, the local environment within the junction differs from duplex DNA in the same sequence context.

To accomplish this, we incorporated 6-MI at ten different locations throughout our HJ model system to gather site-specific information. Fluorescence lifetime measurements, the relative brightness and fluorescence anisotropy at each location, along with fluorescence quenching assays demonstrated that structural distortions imposed by strand exchange results in increased solvent exposure, reduced stacking interactions between bases, and greater extrahelicity at the junction core. Molecular dynamics simulations using a model HJ further suggested that the source of deformation is primarily in the shift and twist parameters of the bases at the junction center and that exchanging strand bases at the HJ center exhibit increased motion. These results which give both base-specific and site-specific information demonstrate the utility of 6-MI for probing nucleic acid structure and dynamics. They further suggest that protein recognition of junctions may be driven by the non-canonical, dynamic structure of the exchanging strand bases at the junction center.

MATERIALS AND METHODS

Sample preparation

6-MI containing oligonucleotides were purchased from Fidelity Oligos LLC (Gaithersburg, MD) in polyacrylamide gel electrophoresis (PAGE)-purified form. High Performance Liquid Chromatography (HPLC)-purified complementary strands were purchased from Integrated DNA Technologies (Coralville, IA). All other reagents were purchased from Sigma-Aldrich (St. Louis, MO) unless otherwise indicated. Single-stranded DNA was stored at -20 °C prior to use. Duplex and HJ DNA were formulated using equal molar amounts of the 6-MI-containing and complementary strands in a 10 mM Tris, pH 8.0 buffer containing 300 mM NaCl and 1 mM EDTA, heating at 75 ºC for 6 hrs followed by slow cooling to room temperature in a water bath.

Steady state fluorescence measurements

The fluorescence intensities of 6-MI-containing J3 samples relative to duplex DNA were measured on a Horiba Fluoromax-4 spectrofluorometer (Edison, NJ) at 10 ºC at 430 nm with a 2 nm bandpass. Intensities were determined from fluorescence emission spectra using an excitation wavelength of 340 nm with a 2 nm bandpass. The fluorescence emission was scanned from 400 to 500 nm at a resolution of 1 nm/pt with an integration of 0.5 s/pt. Ratios were determined from peak intensity values of the J3 substrate spectrum divided by those obtained from the equivalent duplex spectrum. Fluorescence anisotropy measurements were carried out with excitation and emission wavelengths of 340 nm and 430 nm, respectively with a 5 nm bandpass. Fluorescence anisotropy ratios were determined in the same manner as intensity ratios. All values were determined from at least three different experiments and errors are reported as the standard deviation.

Each DNA substrate was prepared in Buffer A (10 mM Tris, pH 7.5, 100 mM NaCl, and 5 mM $MgCl_2$) to a final concentration of 200 nM.

Fluorescence quenching assays

KI was titrated from 0 to 160 mM into a 400 nM solution of 6-MI-containing duplex or HJ DNA. The ionic strength of the solution was held constant at 200 mM K^+ by balancing the KI and the KCl concentrations in a 10 mM Tris, pH 7.5 buffer. Samples were excited at 340 nm and background-corrected emission was collected at 430 nm both with a 3 nm bandpass with a 5 s integration at 10 °C.

The quencher accessible fraction was determined from non-linear curve-fitting of the data using a modified Stern-Volmer equation [31]:

$$I = \frac{I_{fa}}{1 + K_{SV}[KI]} + I_0 - I_{fa} \quad (1)$$

where I represents the intensity, I_0 represents the initial intensity, I_{fa} is the intensity of the quencher accessible fraction, and K_{SV} is the Stern-Volmer constant. The quencher accessible fraction (f_a) was calculated from the average of three separate experiments and the error is the standard deviation.

Time-resolved fluorescence lifetime measurements

Time-correlated single-photon counting (TCSPC) was performed using a Photon Technology International TimeMaster instrument. Samples containing 100-300 nM DNA were prepared in Buffer A and excited with a 375 nm pulsed picosecond diode laser with a repetition rate of 1 MHz (Becker & Hickl). Fluorescence emission was detected at 460 nm with emission slits set at a 20 nm bandpass using a 450 nm cutoff filter and an emission polarizer set to 54.7°. During measurement, all samples were stirred and maintained at 10 °C. Integrity of the samples was verified post irradiation through native gel electrophoresis [28]. Decays were collected over a 55 ns time range with 4096 channels until a maximum of 20000 counts was obtained in the peak channel. The instrument response function was collected by measuring scattered light from a colloidal suspension of Ludox (Sigma Aldrich). The lifetime decays were fit to a sum of exponentials using the following equation:

$$I(t) = \sum_{i=1}^{n} \alpha_i e^{-(\frac{t}{\tau_i})} \quad (2)$$

where $I(t)$ is the intensity at time t, and α_i is the amplitude of the ith component and represents the fractional population with a lifetime of τ_i. Fitting and analysis were performed using either Globals Unlimited [32] or FelixGX (Photon Technologies International) software. Goodness of fit was determined through examination of residuals and chi-squared values in the 0.9-1.3 range. DEF substrates were fit to a sum of two exponentials and all other substrates required three exponentials for fitting. The intensity-weighted mean fluorescence lifetimes (τ_f) and relative amplitudes α_i were calculated from the fits and are averaged from three independent experiments using the following expressions:

$$\tau_f = \frac{\sum_i \alpha_i \tau_i^2}{\sum_i \alpha_i \tau_i} \quad (3)$$

$$\alpha_i = \frac{\alpha_i}{\sum_i \alpha_i} \quad (4)$$

Molecular dynamics setup and analysis

Coordinates for the starting HJ structure were obtained from Prof. Wilma Olson (Rutgers University) [33]. Molecular dynamics (MD) simulations for the J3 HJ were performed using the GPU PMEMD version of AMBER 16.0 and AMBER 18.0 suite of programs with the parmbsc1 forcefield for the DNA [34-36]. The system was solvated using a TIP3P [37] water model in a 12.0 Å octahedral box with Na^+ or K^+ ions to a final concentration of 100 mM NaCl or KCl. The particle mesh Ewald algorithm [38, 39] and a 10 Å Lennard-Jones cutoff were used to treat long-range electrostatic interactions. Initial calculations were energy minimized with four separate minimizations of 1000 steepest descent (SD) and 500 conjugate gradient (CG) steps with harmonic constraints of 100, 100, 10, 0 kcal/mol on solute and 20, 0, 0, 0 kcal/mol on the ions. This was followed by slow heating to 300 K, and four separate equilibrations of 10 ps steps with harmonic constraints of 25, 25, 15, 5 kcal/mol on solute and 20, 20, 10, 0 kcal/mol on the ions. The production steps were performed in conjunction with constant number of particles, constant pressure

and constant temperature (NPT) ensemble conditions and Berendsen algorithm [40]. The SHAKE [41] constraints were applied to all the bonds including hydrogen bonds with an integration time of 2 fs and the trajectory snapshots were saved every 2 ps until the final MD simulation time was reached.

Stability and convergence of the simulations were assessed with root mean-square deviations (RMSD) with respect to the average structure. The 3DNA webserver was used to calculate the helical parameters for the average structure obtained from the MD simulations [42]. Root mean square fluctuations (RMSF) by residue were obtained using the CPPTRAJ RMSF command with time frames of 200 ps using the average structure as reference [43]. The RMSF was calculated using a sliding window of three bases as a means for estimating the local motion of the middle base with respect to its adjacent neighbors. The center of mass for each nucleotide base was determined using PyMol [44]. Distances between the center of mass for adjacent bases were measured using the average structure. The B-DNA reference was generated by analyzing a homoduplex DNA crystal structure (PDB: 1BNA) in the same manner [45].

RESULTS

To understand the structural features that lead to protein recognition and processing of the four-stranded branched DNA molecules known as four-way or Holliday junctions (HJ), we compared the environment of DNA bases within the arms and center of HJs relative to duplex DNA. To ensure that we maintained the same sequence context, 34 bp 6-MI-containing strands were annealed with corresponding complementary strands to form either duplex or HJ DNA (Table S1). We used ten different 6-MI probe positions to observe single base dynamics at distinct locations in the well-characterized J3 HJ. The J3 junction exists primarily in the iso-II conformation (80%) and we use this conformation for designating the continuous and exchanging strands. Nevertheless, we note that 20% of the population is in the iso-I conformation, implying that any effects observed are likely stronger than detected [6-12]. Herein, we identify specific positions by indicating the junction strand followed by the position from the 5’ end. For example, X8 indicates the 6-MI probe is in the X strand and at base position 8 from the 5’ end. Residue positions, 8, 11, and 12 are located in junction arm positions, which are expected to be most like canonical B-DNA (Fig. 1A) [17, 46]. Positions 16 through 19 in the B strand of J3 are all guanines and are substituted with 6-MI giving us access to bases at the junction center (positions 17 and 18) and one position from the center (positions 16 and 19) on an exchanging strand without changing the sequence. In addition, guanines at position 19 on the H strand and 16 on the X strand are used to probe positions one base from the center on continuous strands (Fig. 1A). By using these positions, we incorporated 6-MI throughout the junction without altering the sequence.

How does the environment of the HJ center compare with the HJ arms?

To probe different locations within the HJs, we employed time-resolved fluorescence spectroscopy and measured the lifetimes of 6-MI probes located in the arms and at the junction center. Fluorescence lifetime decays were well-described by a sum of exponentials in which three lifetime components, short (0.1-0.7 ns), medium (1-4 ns), and long (5-8 ns), were needed to fit the decays (Supporting Information: Fig. S1). The short lifetime component arises from 6-MI stacking with adjacent bases, the long lifetime component is attributed to an extrahelical conformation, while the medium lifetime component is assigned to an intermediate conformation [22, 23, 47, 48]. (Fig. 1C). The relative amplitude of each component corresponds to the fractional population of that component. We used these fractional populations to compare the differences in probe environment in the different junction locations. When 6-MI is incorporated into junction arms, the fractional population of the long component is greatly reduced, and most of the decay is described by short and mid-range lifetime components. This is consistent with a probe environment where the fluorescence is mainly quenched through stacking and collisional interactions with adjacent bases. In contrast, when 6-MI is incorporated at the HJ center, an increase in population of the long lifetime component and a decrease in population of the short component led to more even

distribution of the fractional populations between the three lifetime components (Fig. 1C). This re-distribution of populations is primarily observed for the probes in the exchanging strands (B16-B19). In the case of probes on the continuous strand (H19 and X16), this effect is less pronounced, and the fractional populations of the long-lived components only increase slightly. As the junction exhibits an 80:20 population distribution for the iso-II and iso-I conformations [6-12] the H19 and X16 probes will be in an exchanging strand for a fraction of the time, possibly leading to the longer lifetimes observed. The increase in population of the long lifetime component probably arises from a reduction in quenching from collisional and stacking interactions with neighboring bases through increased sampling of an extrahelical, solvent-exposed state. At the HJ center, bases on the exchanging strands experience torsional strain when in the stacked-X conformation and are more likely to adopt an extrahelical conformation to relieve the strain as discussed below.

We incorporated the previously characterized duplex-enhanced fluorescence (DEF) sequence ATFAA [22, 23] (F = 6-MI) into either the HJ arms (X8) or center (X17) to observe this effect with greater sensitivity (Fig. 1D). In the arm of the junction, which resembles duplex DNA, we anticipated that probe dynamics would be similar to those previously determined where we found the ATFAA sequence stabilized the 6-MI probe and reduced collisional quenching, resulting in an increase in fluorescence intensity upon duplex formation [23]. In contrast, when 6-MI is placed into the X8 arm position, we observed an approximately 20% decrease in fluorescence intensity (Fig. 1E) relative to the duplex control. We attribute this intensity decrease to a disruption of the DNA structure that rigidly holds the probe in place and keeps it from interacting with neighboring bases. When 6-MI is placed in the HJ center within the ATFAA sequence we detect an approximately 35% decrease in fluorescence intensity compared to homoduplex DNA (Fig. 1E). This larger decrease relative to that observed in the arms is suggestive of a greater loss of rigidity in the B-DNA structure, consistent with more collisional quenching and increased probe motion. While 6-MI in the DEF sequence experiences some loss of structural stability in the HJ arm, the even larger decrease in fluorescence intensity observed for the X17 position is suggestive of greater flexibility in base structure in the HJ center relative to the arm.

Molecular dynamics simulations reveal structural perturbations and increased dynamics at HJ center

To better interpret our fluorescence results, we performed MD simulations on a J3 junction model to gain detailed structural information resulting from the MD trajectories. We used the DNA analysis tool, 3DNA [42, 49] to analyze the MD average structure and compared helical parameters of junction bases with canonical B-form DNA. Twist and shift base pair step parameters calculated from 3DNA are shown for a 1μs simulation performed in NaCl (Fig. 2A) and a 100 ns simulation in KCl (Supporting Information: Fig. S2). In both simulations, the center junction bases exhibit substantial deviations from the average simulated structure. The core base step bridging positions 17 and 18 on either side of the junction center exhibit sharp changes in structure in which the twist changes by as much as 20 degrees and the shift by ± 1 Å relative to canonical values. As the bases get farther away from the center, the base pair steps more closely resemble B-DNA. We found that analysis of both simulations yielded similar trends suggesting that the ion identity did not significantly impact the results.

Root-mean-square fluctuations (RMSF) were calculated for bases throughout the HJ to determine if base dynamics at the junction center are increased relative to other positions. The RMSF was calculated using AMBER CPPTRAJ [43] and a sliding window of three bases to reduce the contribution of larger global motions of the HJ and focus on local motions of the middle base within the context of the two nearest neighbors. Because of the common effect of end fraying, the terminal bases of the DNA strands were not included [50]. Interestingly, the RMSF analysis shows that there is increased motion for positions 16, 17, and 18, but only for the exchanging strands B and R (Fig. 2B). The increased motion of bases in the exchanging strands observed in this analysis is

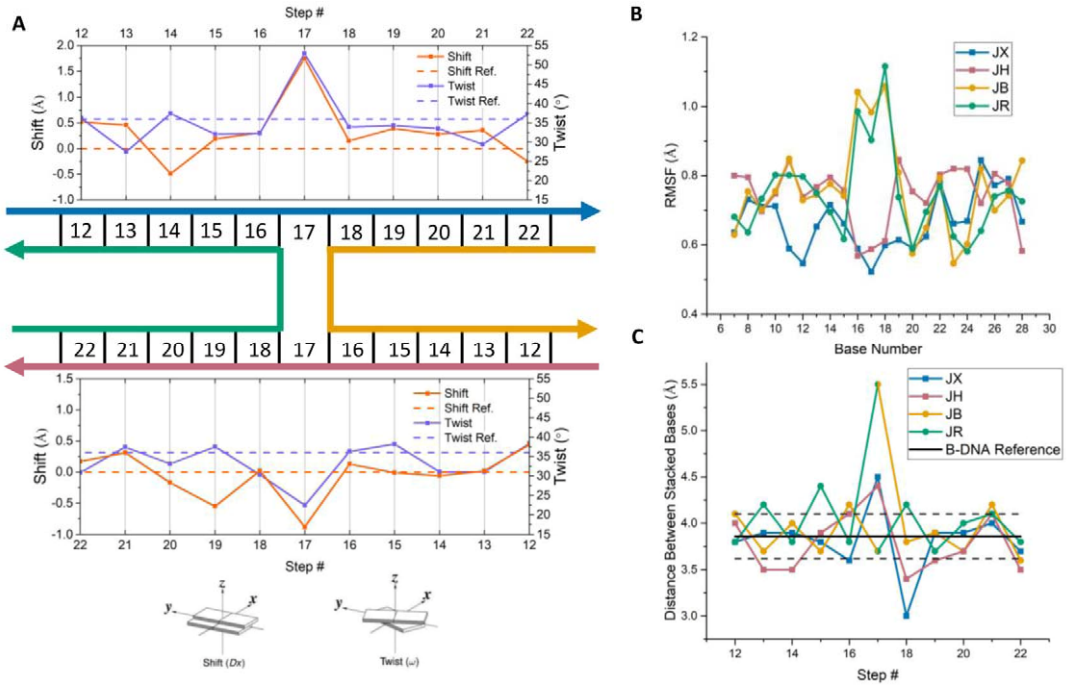

Fig. 2. MD simulations of J3 HJ reveal structural perturbations and increased dynamics at the center. (A) Analyses of a 1 μs simulation revealed deviations in the twist (purple) and shift (orange) base pair step parameters of J3 (solid line) from B-form DNA (dashed line). Step 17 at the HJ center exhibits the largest deviations. Analyses were performed using the 3DNA webserver [42]. (B) Root-mean-square fluctuations (RMSF) over the entire simulation are shown for bases in the JX (blue), JH (red), JB (yellow) and JR (green) strands. The RMSF values were calculated as described in the text. The greatest fluctuations were detected for bases at the HJ center in the exchanging strands (JB and JR, yellow and green, respectively). (C) Distances between the center of mass for adjacent bases at each base step in the average MD structure; HJ center steps 17, 18 are greater than those determined for B-DNA. Strand coloring as shown in (A). B-DNA reference (black) with standard deviation is indicated by dashed lines.

consistent with the increased population of the extrahelical state observed in our fluorescence lifetime measurements. We estimated stacking interactions by examining the distances between the center of mass of the DNA bases and compared the values with similar measurements performed on standard B-form DNA. These analyses are consistent with those of the shift, twist and RMSF, where bases at the center deviate significantly from standard values (Fig. 2C). Cumulatively, the MD results, which indicate bases at the center are significantly distorted from B-form DNA, are consistent with our spectroscopic results and all together suggest that the DNA bases at the HJ center deviate substantially from canonical B-form DNA in structure. These findings are consistent with previous MD simulations of HJs with different DNA sequences in which distortions in twist and shift parameters for bases at the HJ center were observed and junction arms had similar helical parameters to B-form DNA [46, 51, 52]. Additionally, coarse-grained simulated melting of J3 shows the center takes the shortest time to melt [53], where the thermostability is inferred from the faster melting of the center relative to the arms, suggesting decreased stability in the center. The lower stability arises in part from weaker stacking interactions at the HJ center which is correlated with increased lability of those bases.

Comparison of junction base structure and dynamics with duplex DNA

To examine the environment and dynamics of individual bases in Holliday junctions, we compared the properties of 6-MI probes in HJs and in homoduplex DNA in the same sequence context, using fluorescence intensity and steady-state

anisotropy. This comparison of fluorescence anisotropies and intensities between junctions and duplexes further indicates increased dynamics of HJ center bases when compared to B-form duplexes. The fluorescence intensity ratios of junction positions relative to duplex with the same sequence are shown in Fig. 3A. These intensity ratios show that the 6-MI probe positions at the HJ center (positions 16-19) are more fluorescent than their duplex counterparts. As the probe is moved out of the center and into the arms of the HJ there is less of a difference in intensity which can be seen by looking at the B12, X11, and X8 positions. Comparing the changes in intensity between probes located at the B16-B19 (exchanging) positions to H19 and X16 (continuous) positions also reveals that this effect is greater for bases in the exchanging strand versus the continuous strand (Fig. 3). Although our results are based on the dominant conformation in solution, we note that the conformation distribution is 80:20 and the minor population will influence the results and possibly lead to the small changes detected for the H19 and X16 probes. We also observed that 6-MI located in the junction center exhibits the same spectral characteristics as when it is located in a loop or adjacent to a mismatch site [23, 28], consistent with a loss of duplex structure and more frequent excursions to extrahelical or single-stranded states. In general, these results indicate that probes at the HJ center are less stacked and experience less collisional quenching from neighboring bases than they would in duplex DNA.

We also compared the local and global motions of the 6-MI probe in different junction locations with duplex DNA through steady-state anisotropy measurements (Fig. 3B), which indicated that the anisotropy of 6-MI in a duplex is higher than in the HJ within the same sequence context. This is surprising, as the junction is larger and should have a longer global rotation time and consequently, higher anisotropy. As the steady-state measurements give a weighted average of local and global motions [31], this finding suggests that the local motions in the junction outweigh the global motions of the HJ. As shown in Fig. 3B, 6-MI anisotropy measurements also revealed that this effect is more pronounced for bases located at the center rather than the arms of HJs. We infer from these results that bases contained in the HJ experience greater local dynamics and less quenching from neighboring bases relative to bases in duplex DNA, particularly at the center.

Fluorescence lifetime measurements of 6-MI probes in HJ or duplex DNA also point to a reduction in quenching interactions for bases located in the HJ.

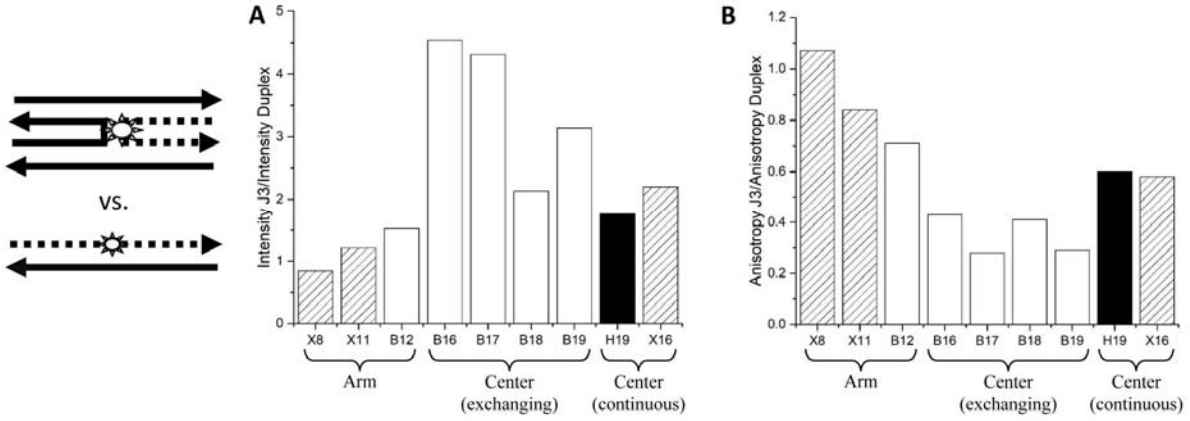

Fig. 3. Ratios of fluorescence intensity (A) and anisotropy measurements (B) for 6-MI containing HJs and duplexes in identical sequence contexts. (A) Increased fluorescence intensity observed for junctions relative to duplex, with the largest differences observed for locations, B16-B19. (B) Lower anisotropy values observed in HJs relative to duplex DNA, with the largest differences at the HJ center (B16-B19). Ratios were determined from at least three measurements. Sample conditions as in Figure 1.

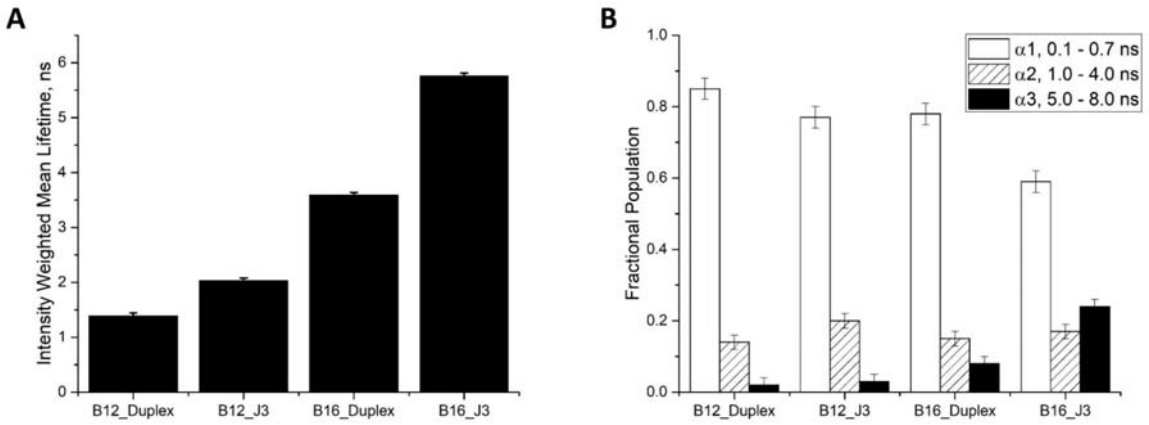

Fig. 4. Fluorescence lifetime measurements comparing HJ and duplex DNA for different HJ positions within the same sequence context. (A) Intensity-weighted fluorescence lifetimes of 6-MI probes were calculated as described in the text and are longest for the B16 probe. (B) Fractional populations of the lifetime components obtained from the fluorescence decays as described in the text. The increase in lifetime at the B16 junction position arises from a shift in fractional population from the shortest lifetime component to the longest. Error bars represent the standard deviation from at least three experiments. Sample conditions as in Figure 1. Decay fit parameters are given in Supporting Information: Table S3.

We observed an increase in the intensity-weighted fluorescence lifetimes (τ_f) in the HJ compared to duplex DNA (Fig. 4A). This effect is more pronounced for the B16 probe compared to the B12 probe, which is consistent with our other measurements that suggested bases at the center experience more motion and are more solvent-exposed relative to bases in the arms. The increase in lifetime for probes located in the junction arms further indicated that the helical structure in the arms is less constrained than in the corresponding duplex, suggesting that the torsional stress induced by the center exchanging strands propagates throughout the junction as suggested by our measurements with the duplex-enhanced fluorescence substrates (Fig. 1E and Fig. S3).

The distribution of fractional populations of the 6-MI fluorescence lifetime components differs between duplex and junction, where an increase in fractional population of the longer-lived components is observed for junction decays (Fig. 4B). Analysis of the B12 probe decay demonstrated that the shift in fractional populations mainly occurred between the short (0.1-0.7 ns) and mid-range (1-4 ns) lifetime components. In the case of the center B16 position, the increase in fractional population of the long-lived component was more pronounced and was three times that of the long-lived component measured in the same sequence context in duplex DNA (Fig. 4B). As the longest lifetime component of the 6-MI probe (5-8 ns) likely arises from a conformation that is more extrahelical in nature and more comparable to the monomer dye, the observed population shift supports our finding that bases in the junction center are less stacked and adopt an extrahelical conformation more frequently.

To verify the extrahelical nature of the center bases, we measured the relative solvent exposure of the 6-MI probe in the junction center and arms (Fig. 5). Quenching of 6-MI fluorescence induced with KI addition provides an estimate of the fluorophore quencher accessible fraction. Comparison of junction data with that from the X11 and B16 duplexes demonstrates that the quencher accessible fraction depends on sequence context. As shown, in duplex DNA, the B16 position leads to greater quencher accessibility of the 6-MI (73%) relative to the X11 sequence (35%) due to the purine nature of the adjacent bases (Table 1) [25, 54]. Nevertheless, a comparison within the same sequence context in the HJ shows that quencher accessibility increased by 13% for the B16 position, while the probe in the X11 position

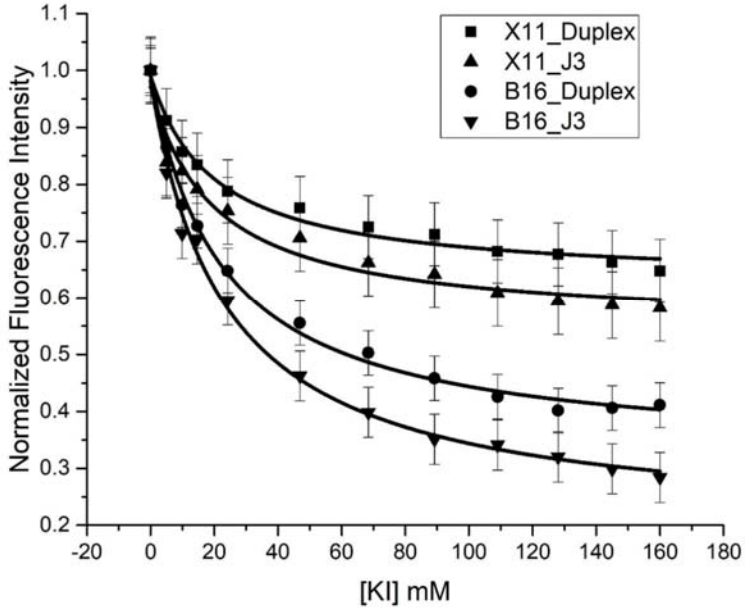

Fig. 5. Accessibility of 6-MI to quencher in HJs compared to duplex DNA within the same sequence context. The difference in the quencher accessible fraction between HJ and duplex DNA is greater for the position at the center of the HJ (B16) than the arm of the HJ (X11), consistent with an increase in extrahelicity of 6-MI at the HJ center. The quencher accessible fraction was determined using a modified Stern-Volmer expression as described in the text.

Table 1. Quencher accessibility of 6-MI in duplex and HJ substrates determined with KI.

DNA Substrate[1]	Quencher Accessible Fraction[2]
B16_Duplex	0.73 ± 0.05
B16_HJ	0.86 ± 0.04
X11_Duplex	0.35 ± 0.06
X11_HJ	0.41 ± 0.09

[1]Letter and number indicate location of probe. [2]The quencher accessible fraction was determined from non-linear curve-fitting of the data using a modified Stern-Volmer equation (Eq. 3) [31] as described in the text.

only experienced half that increase in accessibility (Table 1) (Fig. 5). The difference in quencher accessibility between the duplex and junction arm is within our range of error, suggesting those environments are comparable, which is not the case for the junction center. Collectively, our fluorescence and simulation results point to an environment in the junction center that is more solvent exposed and exhibits greater dynamics than either the junction arms or the corresponding duplexes.

DISCUSSION

A dynamic and flexible junction center

Time-resolved and steady-state fluorescence emission measurements coupled with MD simulations have yielded new information on the local structure and dynamics of a 34 bp DNA Holliday junction. This information points to a distorted central junction region in which individual bases adopt extrahelical conformations more often and consequently, experience reduced stacking interactions. Furthermore, our findings show that bases in the junction exchanging strands experience greater perturbations in local structure relative to those in the continuous strands. These unique structural properties of bases at the junction center provide a potential avenue through which proteins both recognize HJs and distinguish the exchanging from the continuous strands.

The current findings are well supported by those obtained with other methods. NMR studies measuring the width of proton resonances have also detected greater conformational flexibility in exchanging strands relative to continuous strands [13-15, 55].

A prior study used circular dichroism and differential scanning calorimetry to infer a reduction in base stacking at the junction center [56]. Significantly, our results both confirm and extend these observations as the 6-MI probe is a more sensitive reporter of local structure and detected reduced base stacking within a helical turn of the center. Overall, these findings suggest that the junction structure at the central core and extending to proximal bases is more dynamic and less constrained than duplex DNA and possibly presents a likely target for protein recognition and binding, as discussed below.

Implications for protein recognition of junction structures

The average structure of our simulated J3 Holliday junction used in this study is depicted in Fig. 6 in comparison with four protein-bound junction structures. Notably, in the protein-junction complexes, the center regions, which are the primary contact point for proteins, are distorted and relatively open with many deviations from canonical B-DNA structure. Our simulated, protein-free J3 structure maintains the stacked-X iso-II conformation, and increased opening at the center is not observed (Fig. 6A). A recent report demonstrated that variations of the standard AMBER forcefields better simulate spontaneous transitions in HJ conformations [57]. Thus, the AMBER bsc1 forcefield could be over stabilizing the central region through increased stacking interactions; however, we do detect extensive distortions and heightened dynamics in the core (Fig. 2; Fig. S2). Undoubtedly, these distortions would be even more pronounced with the use of the specialized forcefields.

The loss of base stacking and in some cases base-pairing in the protein-bound structures (Fig. 6B-E) suggests that flexibility at the core is an important recognition mechanism for junction-binding proteins [17, 20, 58]. For example, in the T7 endonuclease I-bound-HJ crystal structure (Fig. 6B), two different conformations for center bases are detected (highlighted in cyan). The base is located in an exchanging strand on the 5' side of the core step, making it equivalent to base 17 (B17 or X17) in our study. The observation of two different protein-bound conformations is consistent with the inherent distortion and flexibility of the B17 and X17 bases measured in our solution assays. Similarly, the open conformation at the center of the P1 Cre recombinase-HJ complex and larger

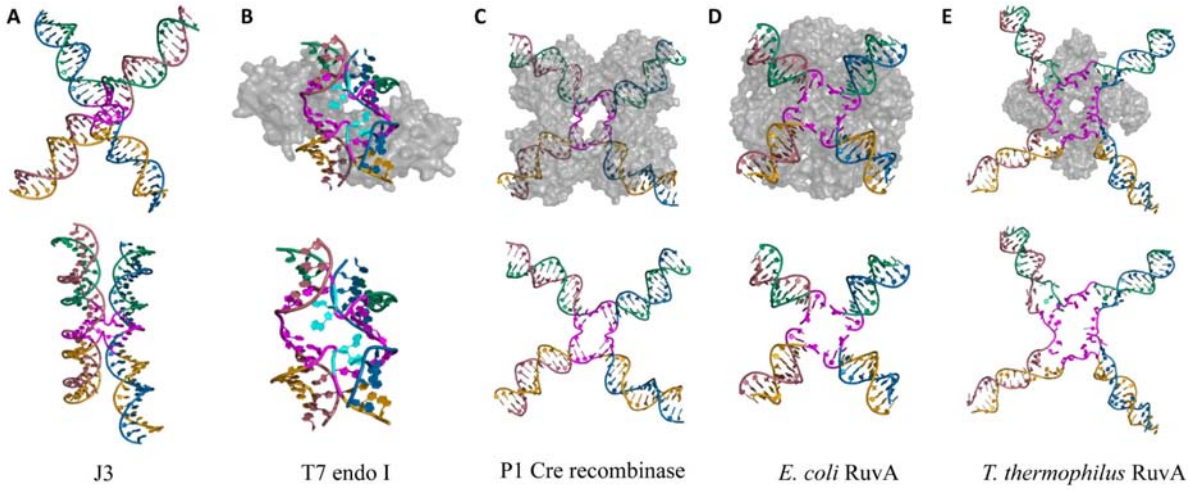

Fig. 6. Structural comparison of free and protein-bound HJs. Strands are color coded to match the J3 junction with the four central bases of each strand highlighted in magenta. (A) J3 HJ average structure obtained from 1μs of MD simulation performed in 100 mM NaCl as described in the text. (B) HJ central bases resolved in two different orientations (cyan) in the T7 endonuclease I (endo I)-bound HJ structure (PDB: 2PFJ). (C) P1 Cre recombinase-bound HJ (PDB: 2QNC), (D) *E. coli* RuvA-bound HJ (PDB: 1C7Y), and (E) *T. thermophilus* RuvA-bound HJ (PDB: 8GH8); all show significant opening and distortion of the junction center with protein bound.

than average thermal parameters in the crossover region of this structure also point to local increased mobility [58]. Opening of the HJ center in the *E. coli* RuvA crystal structure [17] and *T. thermophilus* RuvA EM structure (PDB:8GH8) is accompanied by base unstacking and unpairing. Thus, these protein-bound junction structures support and confirm our findings that the junction core represents a labile and dynamic region, in which excursions to extrahelical states potentially facilitate recognition and binding.

In previous work, 6-MI has been shown to be a sensitive reporter of DNA structure either alone or in complex with proteins [22, 23, 25, 26, 28, 59, 60]. Our study further supports and extends these findings as subtle changes in junction structure, undetected by other methods, were reflected through 6-MI fluorescence properties. This sensitivity to junction structure, makes 6-MI a useful probe for studying protein-junction interactions.

CONCLUSION

We have used 6-MI to investigate local structure and dynamics of DNA bases in HJs. Through time-resolved and steady-state fluorescence measurements and MD simulations we have shown that the structural distortions imposed by strand crossing result in increased solvent exposure, less stacking of bases and greater extrahelical nature of bases within the junction core. Furthermore, these studies show that bases in the exchanging strands are more labile than those in the continuous strands. These deviations from standard B-form DNA suggest a mechanism through which junction-binding proteins may recognize HJs and discriminate between strands. The current study also confirms the usefulness of 6-MI for investigating DNA structure and dynamics. As HJs are attractive drug targets for cancer therapies [1], we suggest that the sensitivity of 6-MI to junction structure, as demonstrated in this report, makes 6-MI an excellent candidate for developing an effective sensor to screen ligand binding to the junction center.

ACKNOWLEDGEMENTS

We thank Prof. Wilma Olson (Rutgers University) for the structural coordinates of the model junctions. This work was supported by National Institutes of Health grant R15GM135904 (awarded to IM).

CONFLICT OF INTEREST STATEMENT

The authors declare no competing financial interest.

SUPPORTING INFORMATION

Table S1. Sequences of DNA oligomers used in this study. F = 6-MI. The letter denotes the strand of the Holliday junction, while the number represents the position of 6-MI from the 5' end. All strands are 34 bp long.

Name	Sequence
JX	5' – CCA GAC TGC AGT TGA GTC CTT GCT AGG ACG GAG G – 3'
JX8	5' – CCA GAA T**F**A AGT TGA GTC CTT GCT AGG ACG GAG G - 3'
JX11	5' – CCA GAC TGC A**F**T TGA GTC CTT GCT AGG ACG GAG G – 3'
JX16	5' – CCA GAC TGC AGT TGA **F**TC CTT GCT AGG ACG GAG G – 3'
JX17	5' – CCA GAC TGC AGT TGA T**F**A ATT GCT AGG ACG GAG G – 3'
JB	5' – CCT CCG TCC TAG CAA GGG GCT GCT ACC GGA AGG G - 3'
JB12	5' - CCT CCG TCC TA**F** CAA GGG GCT GCT ACC GGA AGG G - 3'

Table S1 continued..

JB16	5’ - CCT CCG TCC TAG CAA **F**GG GCT GCT ACC GGA AGG G - 3’
JB17	5’ - CCT CCG TCC TAG CAA G**F**G GCT GCT ACC GGA AGG G - 3’
JB18	5’ - CCT CCG TCC TAG CAA GG**F** GCT GCT ACC GGA AGG G - 3’
JB19	5’ - CCT CCG TCC TAG CAA GGG **F**CT GCT ACC GGA AGG G - 3’
JB_X17_Comp	5’ – CCT CCG TCC TAG CAA TTG GCT GCT ACC GGA AGG G - 3’
JH	5’ – CCC TTC CGG TAG CAG CCT GAG CGG TGG TTG AAG G – 3’
JH19	5’ - CCC TTC CGG TAG CAG CCT **F**AG CGG TGG TTG AAG G - 3’
JR	5’ – CCT TCA ACC ACC GCT CAA CTC AAC TGC AGT CTG G – 3’
JR_X8_Comp	5’ - CCT TCA ACC ACC GCT CAA CTC AAC TTC ATT CTG G - 3’
JR_X17_Comp	5’ – CCT TCA ACC ACC GCT CAC ATC AAC TGC AGT CTG G – 3’
JH_Duplex_Comp	5’ – CCT TCA ACC ACC GCT CAG GCT GCT ACC GGA AGG G – 3’
JR_Duplex_Comp	5’ – CCA GAC TGC AGT TGA GTT GAG CGG TGG TTG AAG G – 3’
JB_Duplex_Comp	5’ – CCC TTC CGG TAG CAG CCC CTT GCT AGG ACG GAG G – 3’
JX_Duplex_Comp	5’ - CCT CCG TCC TAG CAA GGA CTC AAC TGC AGT CTG G – 3’
X8_HD	5’ - TAT GCA GTC ACT AT**F** AAT CAA CTA CTT AGA TGG T - 3’
X8_HD_Comp	5’ - ACC ATC TAA GTA GTT GAT TCA TAG TGA CTG CAT A - 3’

Table S2. Time-resolved fluorescence decay parameters for Holliday Junctions containing 6-MI.

DNA Substrate[1]	α_1 [2]	τ_1	α_2 [2]	τ_2	α_3 [2]	τ_3	τ_f [3]
X11_J3	0.47	0.63	0.48	1.59	0.05	6.89	2.75
B12_J3	0.77	0.50	0.20	1.38	0.03	6.28	2.03
B16_J3	0.59	0.45	0.17	2.7	0.24	7.4	5.47
B17_J3	0.42	0.43	0.28	2.58	0.31	6.98	5.55
B18_J3	0.46	0.47	0.26	2.98	0.28	7.07	5.53
B19_J3	0.45	0.67	0.32	3.74	0.23	7.71	5.59
H19_J3	0.8	0.54	0.14	1.83	0.06	5.78	2.57
X16_J3	0.84	0.29	0.09	1.88	0.07	6.11	3.4

[1]Letter and number indicate location of probe in the J3 junction. [2]Relative amplitudes are calculated from the decays as follows: $\alpha_i = \frac{\alpha_i}{\sum_i \alpha_i}$. [3]$\tau_f$ is the intensity-weighted mean lifetime defined as $\tau_f = \frac{\sum_i \alpha_i \tau_i^2}{\sum_i \alpha_i \tau_i}$.

Table S3. Time-resolved fluorescence decay parameters for Holliday Junction or duplex DNA containing 6-MI in the same sequence context.

DNA Substrate[1]	α_1[2]	τ_1	α_2[2]	τ_2	α_3[2]	τ_3	τ_f[3]
6-MI Monomer	-	-	-	-	1.00	6.52	6.52
X8_Duplex	-	-	0.1	3.47	0.9	7.33	7.14
X8_J3	-	-	0.17	2.81	0.83	6.82	6.53
B12_Duplex	0.85	0.53	0.14	1.48	0.02	5.84	1.39
B12_J3	0.77	0.50	0.20	1.38	0.03	6.28	2.03
B16_Duplex	0.78	0.63	0.15	2.2	0.08	7.05	3.59
B16_J3	0.59	0.45	0.17	2.7	0.24	7.4	5.76

[1]Letter and number indicate location of probe in either junction or duplex DNA. [2]Relative amplitudes reported as $\alpha_i = \frac{\alpha_i}{\sum_i \alpha_i}$. [3]$\tau_f$ is the intensity-weighted mean lifetime defined as $\tau_f = \frac{\sum_i \alpha_i \tau_i^2}{\sum_i \alpha_i \tau_i}$.

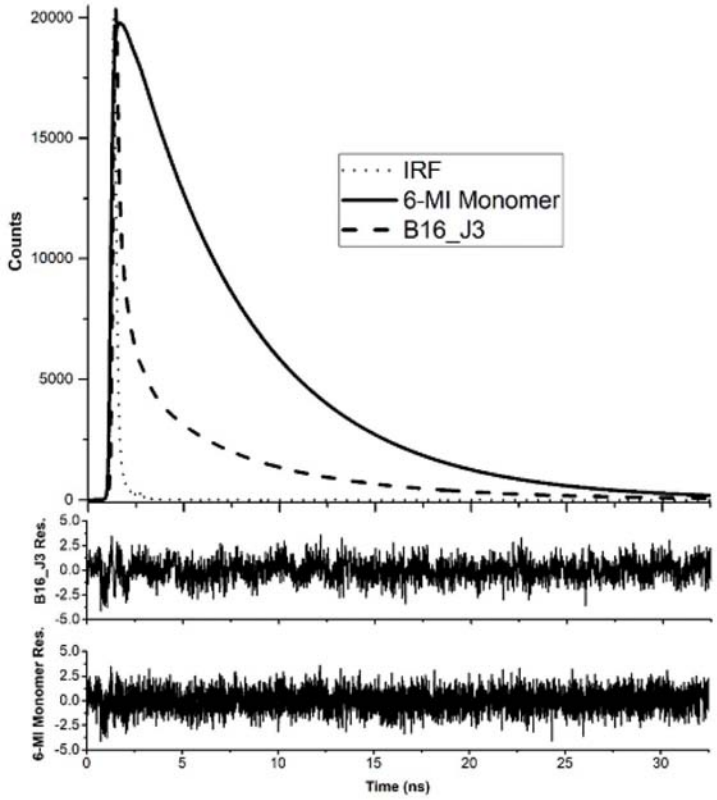

Fig. S1. Top: Representative fluorescence lifetime decays of 6-MI monomer (solid line) and B16_J3 (dashed line) with instrument response function (dotted line). Fluorescence lifetime decays were fit to a sum of exponentials as described in the text. Decays were collected until a maximum of 20000 counts was obtained in the peak channel as described in the text. Bottom: The bottom trace depicts the residuals between the fit and the decay. Samples contained 200 nM 6-MI monomer or 6-MI-containing DNA in a 10 mM Tris, pH 7.5, 100 mM NaCl and 5 mM $MgCl_2$ buffer. Fit parameters are given in Supporting Information: Table S2.

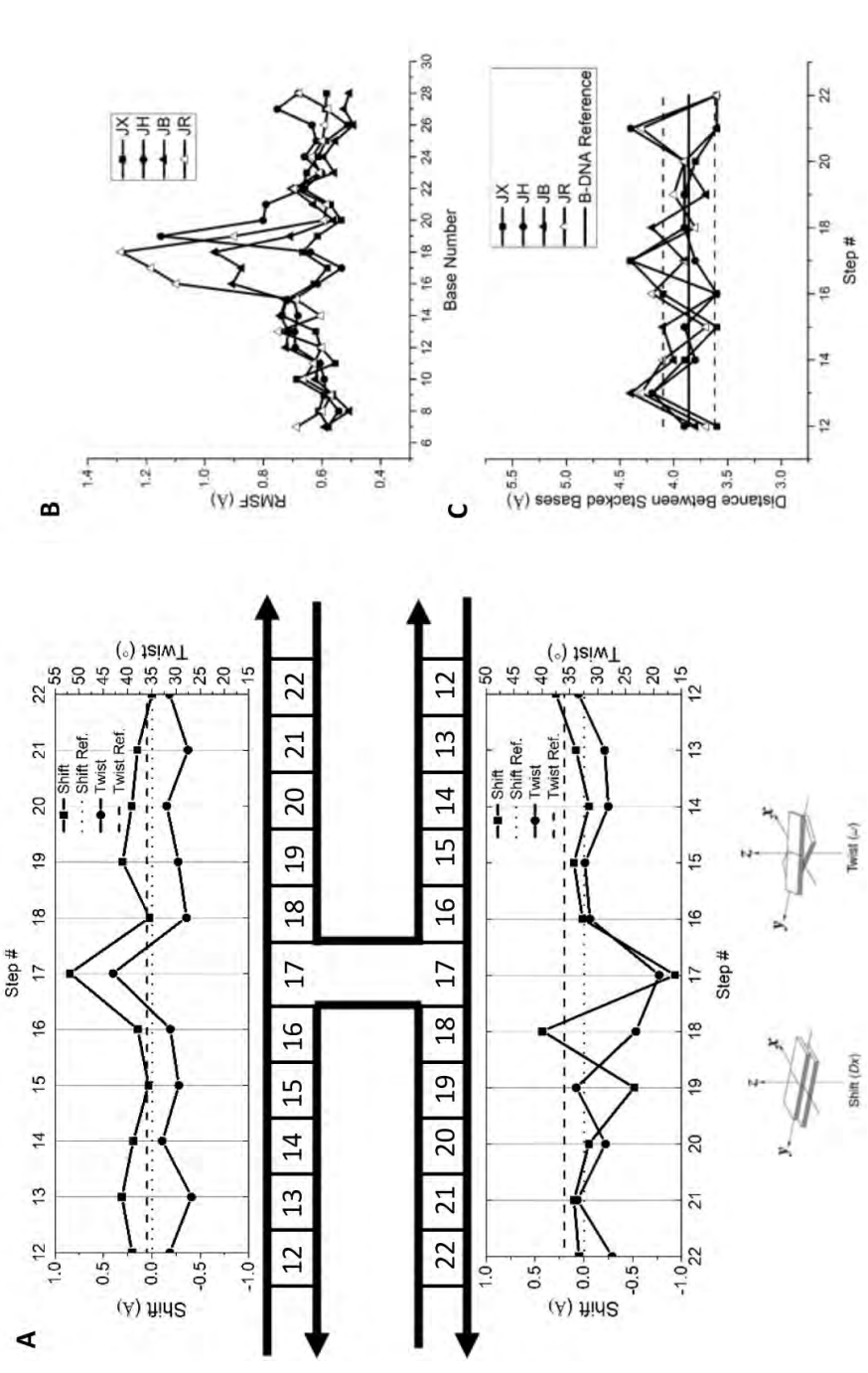

Fig S2. Molecular dynamics simulations of the J3 HJ reveal structural perturbations and increased dynamics at HJ centers. (A) Analyses of a 100 ns simulation were performed using the 3DNA webserver [42] and revealed deviations in the twist and shift base pair step parameters of J3 from canonical B-form DNA. Canonical B-DNA values are shown with a dashed line and J3 parameters are depicted with a solid line. Step 17 at the HJ center exhibits the largest deviations. (B) Root-mean-square fluctuations (RMSF) throughout the course of the simulation are shown for bases in the JX, JH, JB and JR strands. The RMSF values were calculated for individual bases using a sliding window of three bases to estimate the local motion of the middle base with respect to its nearest neighbors. The greatest fluctuations were detected for bases at the center of the HJ in the exchanging strands (JB and JR). (C) Distances between the center of mass of adjacent bases at each step in the average MD structure. The distance between bases at the HJ center is greater than the average value determined for B-DNA. The standard deviation for the B-DNA reference is shown by the black dashed lines.

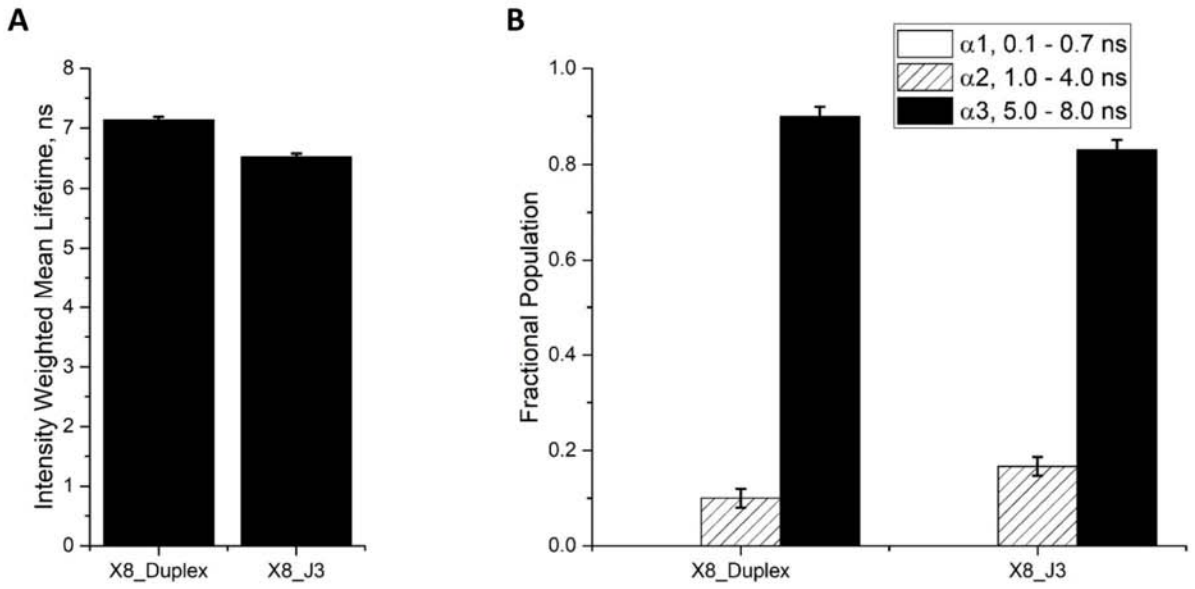

Fig. S3. Fluorescence lifetime measurements comparing the DEF sequence in HJ and duplex DNA. (A) Intensity-weighted mean fluorescence lifetimes for 6-MI probes in HJs and duplex DNA within the enhanced fluorescence ATFAA sequence context. (B) Fractional populations of the lifetime components obtained by analyzing fluorescence lifetime decays to a sum of exponentials as described in the text. In this sequence context, shorter lifetimes are observed for the HJ, as the structural constraints of the DEF sequence structure are released, and more dynamic quenching is observed. Samples included 200 nM DNA in a 10 mM Tris pH 7.5, 100 mM NaCl and 5 mM $MgCl_2$ buffer. Fit parameters are given in Supporting Information: Table S3.

REFERENCES

1. Song, Q., Hu, Y., Yin, A., Wang, H. and Yin, Q. 2022, Int. J. Mol. Sci., 23, 9730.
2. Liu, Y. and West, S. C. 2004, Nat. Rev. Mol. Cell Biol., 5, 937.
3. Wyatt, H. D. and West, S. C. 2014, Cold Spring Harb. perspect. biol., 6, a023192.
4. Lilley, D. M. J. 2017, FEBS Lett., 591, 1073.
5. Murchie, A. I., Clegg, R. M., von Kitzing, E., Duckett, D. R., Diekmann, S. and Lilley, D. M. 1989, Nature, 341, 763.
6. Clegg, R. M., Murchie, A. I. H. and Lilley, D. M. J. 1994, Biophys. J., 66, 99.
7. Duckett, D. R., Murchie, A. I. H. and Lilley, D. M. J. 1990, The EMBO Journal, 9, 583
8. Duckett, D. R., Murchie, A. I. H., Diekmann, S., Kitzing, E. V., Kemper, B. and Lilley, D. M. J. 1988, Cell, 55, 79.
9. Vitoc, C. I. and Mukerji, I. 2011, Biochemistry, 50, 1432.
10. McKinney, S. A., Declais, A. C., Lilley, D. M. and Ha, T. 2003, Nat. Struct. Biol., 10, 93.
11. Joo, C., McKinney, S. A., Lilley, D. M. and Ha, T. 2004, J. Mol. Biol., 341, 739.
12. Clegg, R. M., Murchie, A. I. H., Zechel, A., Carlberg, C., Diekmann, S. and Lilley, D. M. J. 1992, Biochemistry, 31, 4846.
13. Pikkemaat, J. A., van den Elst, H., van Boom, J. H. and Altona, C. 1994, Biochemistry, 33, 14896.
14. Overmars, F. J., Lanzotti, V., Galeone, A., Pepe, A., Mayol, L., Pikkemaat, J. A. and Altona, C. 1997, Eur. J. Biochem., 249, 576.
15. Chen, S. M. and Chazin, W. J. 1994, Biochemistry, 33, 11453.
16. Miick, S. M., Fee, R. S., Millar, D. P. and Chazin, W. J. 1997, Proc. Natl. Acad. Sci. USA, 94, 9080.
17. Ariyoshi, M., Nishino, T., Iwasaki, H., Shinagawa, H. and Morikawa, K. 2000, Proc. Natl. Acad. Sci. USA, 97, 8257.
18. Zhou, R., Yang, O., Declais, A. C., Jin, H., Gwon, G. H., Freeman, A. D. J., Cho, Y., Lilley, D. M. J. and Ha, T. 2019, Nat. Chem. Biol., 15, 269.

19. Biertumpfel, C., Yang, W. and Suck, D. 2007, Nature, 449, 616.
20. Hadden, J. M., Declais, A. C., Carr, S. B., Lilley, D. M. and Phillips, S. E. 2007, Nature, 449, 621.
21. Snowden, T., Acharya, S., Butz, C., Berardini, M. and Fishel, R. 2004, Mol. Cell, 15, 437.
22. Moreno, A., Knee, J. and Mukerji, I. 2012, Biochemistry, 51, 6847.
23. Moreno, A., Knee, J. L. and Mukerji, I. 2016, J. Phys. Chem. B, 120, 12232.
24. Driscoll, S. L., Hawkins, M. E., Balis, F. M., Pfleiderer, W. and Laws, W. R. 1997, Biophys. J., 73, 3277.
25. Wojtuszewski Poulin, K., Smirnov, A. V., Hawkins, M. E., Balis, F. M. and Knutson, J. R. 2009, Biochemistry, 48, 8861.
26. Mariam, J., Krishnamoorthy, G. and Anand, R. 2019, Chem. Asian J., 14, 4760.
27. Singleton, S. F., Roca, A. I., Lee, A. M. and Xiao, J. 2007, Tetrahedron, 63, 3553.
28. Li, Y., Lombardo, Z., Joshi, M., Hingorani, M. M. and Mukerji, I. 2019, Int. J. Mol. Sci., 20.
29. Adams, N. M., Wang, K. K., Caprioli, A. C., Thomas, L. C., Kankia, B., Haselton, F. R. and Wright, D. W. 2014, Analyst, 139, 1644.
30. Han, J. H., Chitrapriya, N., Lee, H. S., Lee, Y. A., Kim, S. K. and Jung, M. J. 2017, Bull. Korean Chem. Soc., 38, 183.
31. Lakowicz, J. R. 2006, "Principles of Fluorescence Spectroscopy" Springer, New York
32. Beechem, J. M. 1989, Chem. Phys. Lipids, 50, 237.
33. Karymov, M. A., Chinnaraj, M., Bogdanov, A., Srinivasan, A. R., Zheng, G., Olson, W. K. and Lyubchenko, Y. L. 2008, Biophys. J., 95, 4372.
34. Ivani, I., Dans, P. D., Noy, A., Perez, A., Faustino, I., Hospital, A., Walther, J., Andrio, P., Goni, R., Balaceanu, A., Portella, G., Battistini, F., Gelpi, J. L., Gonzalez, C., Vendruscolo, M., Laughton, C. A., Harris, S. A., Case, D. A. and Orozco, M. 2016, Nat. Methods, 13, 55.
35. Case, D. A., Betz, R. M., Cerutti, D. S., Cheatham, T. E., Darden, T. A., Duke, R. E., Giese, T. J., Gohlke, H., Goetz, A. W., Homeye, N., Izadi, S., Janowski, P., Kaus, J., Kovalenko, A., Lee, T. S., LeGrand, S., Li, P., Lin, C., Luchko, T., Luo, R., Madej, B., Mermelstein, D., Merz, K. M., Monard, G., Nguyen, H., Nguyen, H. T., Omelyan, I., Onufriev, A., Roe, D. R., Roitber, A., Sagui, C., Simmerling C. L., Botello-Smith, W. M., Swails, J., Walker, R. C., Wang, J., Wolf, R. M., Wu, X., Xiao, L. and Kollman, P. A. 2016, "AMBER 2016" University of California, San Francisco
36. Case, D. A., Ben-Shalom, I. Y., Brozell, S. R., Cerutti, D. S., Cheatham, T. E., Cruzeiro, V. W. D., Darden, T. A., Duke, R. E., Ghoreishi, D., Gilson, M. K., Gohlke, H., Goetz, A. W., Greene, D., Harris, R., Homeyer, N., Huang, Y., Izadoi, S., Kovalenko, A., Kurtzman, T., Lee, T.S., LeGrand, S., Li, P., Lin, C., Liu, J., Luchko, T., Luo, R., Mermelstein, D. J., Merz, K. M., Miao, Y., Monard, G., Nguyen, C., Nguyen, H., Omelyan, I., Onufriev, A., Pan, F., Qi, R., Roe, D. R., Roitberg, A., Sagui, C., Schott-Verdugo, S., Shen, J., Simmerling, C.L., Smith, J., Salomon-Ferrer, R., Swails, J., Walker, R. C., Wang, J., Wei, H., Wolf, R. M., Wu, X., Xiao, L., York, D. M. and Kollman, P. A. 2018, "AMBER 2018" University of California, San Francisco
37. Jorgensen W. L. C. J., Madura J. D., Impey R. W. and Klein, M. L. 1983, J. Chem. Phys., 79, 926.
38. Essmann, U., Perera, L., Berkowitz, M. L., Darden, T., Lee, H. and Pedersen, L. G. 1995, J. Chem. Phys., 103, 8577.
39. Darden, T., York, D. and Pedersen, L. 1993, J. Chem. Phys., 98, 10089.
40. Berendsen, H. J. C., Postma, J. P. M., van Gunsteren, W. F., DiNola, A. and Haak, J. R. 1984, J. Chem. Phys., 81, 3684.
41. Ryckaert, J.-P., Ciccotti, G. and Berendsen, H. J. C. 1977, J. Comput. Phys., 23, 327.
42. Li, S., Olson, W. K. and Lu, X. J. 2019, Nucleic Acids Res., 47, W26.
43. Roe, D. R. and Cheatham, T. E. 2013, J. Chem. Theory Comput., 9, 3084.
44. The PyMOL Molecular Graphics System, Schrödinger, LLC.
45. Drew, H. R., Wing, R. M., Takano, T., Broka, C., Tanaka, S., Itakura, K. and Dickerson, R. E. 1981, Proc. Natl. Acad. Sci. USA, 78, 2179.

46. Adendorff, M. R., Tang, G. Q., Millar, D. P., Bathe, M. and Bricker, W. P. 2022, Nucleic Acids Res., 50, 717.
47. Hawkins, M. E. 2001, Cell Biochem. Biophys., 34, 257.
48. Hawkins, M. E., Pfleiderer, W., Balis, F. M., Porter, D. and Knutson, J. R. 1997, Anal. Biochem., 244, 86.
49. Lu, X.-J. and Olson, W. K. 2008, Nature Protocols, 3, 1213.
50. Zgarbova, M., Otyepka, M., Sponer, J., Lankas, F. and Jurecka, P. 2014, J. Chem. Theory Comput., 10, 3177.
51. Wheatley, E. G., Pieniazek, S. N., Vitoc, I., Mukerji, I. and Beveridge, D. L. 2012, Innovations in Biomolecular Modeling and Simulations, 2, 111.
52. Wheatley, E. G., Pieniazek, S. N., Mukerji, I. and Beveridge, D. L. 2012, Biophys. J., 102, 552.
53. Kipnis, A. 2019, [Honors Thesis, Wesleyan University],
54. Ahmad, S. 2009, Gene, 428, 25.
55. Pikkemaat, J. A., Overmars, F. J., Dreef-Tromp, C. M., van den Elst, H., van Boom, J. H. and Altona, C. 1996, J. Mol. Biol., 262, 349.
56. Carr, C. E. and Marky, L. A. 2017, J. Am. Chem. Soc., 139, 14443.
57. Zhang, Z., Sponer, J., Bussi, G., Mlynsky, V., Sulc, P., Simmons, C. R., Stephanopoulos, N. and Krepl, M. 2023, J. Chem. Inf. Model, 63, 2794.
58. Gopaul, D. N., Guo, F. and Van Duyne, G. D. 1998, EMBO J., 17, 4175.
59. Lahiri, S., Li, Y., Hingorani, M. M. and Mukerji, I. 2018, Biophys. J., 115, 2087.
60. Datta, K., Johnson, N. P., Villani, G., Marcus, A. H. and von Hippel, P. H. 2012, Nucleic Acids Res., 40, 1191.